Asian Journal of Chemistry; Vol. 37, No. 11 (2025), 2865-2875
ASIAN JOURNAL OF CHEMISTRY
https://doi.org/10.14233/ajchem.2025.34393

Treatment of Oily Wastewater Using Chitosan as Biosorbent: Biosorbent Synthesis and Kinetic Models Evaluation

G.E. NGCOBO, S.M. KHUMALO*, B.F. BAKARE and S. RATHILAL

Green Engineering Research Group, Department of Chemical Engineering, Durban University of Technology, 121 Steve Biko, Musgrave, Durban, South Africa

*Corresponding author: E-mail: SiphesihleK1@dut.ac.za

Received: 3 July 2025 *Accepted*: 10 October 2025 *Published online*: 27 October 2025 AJC-22177

The discharge of untreated oily wastewater is a serious environmental concern, as it contaminates water bodies, threatens aquatic life and disrupts ecosystems. The present study investigates the effectiveness of synthesized oyster-derived chitosan as a biosorbent for the removal of phenol, chemical oxygen demand (COD) and colour from raw oily wastewater emanating from a petrochemical refinery plant. The study recorded 98% phenol, 94% COD and 92% colour reduction at pH 7, contact time of 90 min and adsorbent dose of 9 g/L. Adsorption kinetic studies suggest that the uptake of phenol follows the pseudo-second order kinetic model, COD uptake follows the pseudo-first order (PFO) kinetic model and colour reduction follows the fractal-like PFO kinetic model. Based on the kinetic studies, it was suggested that the treatment of oily wastewater using chitosan is a complex process that involves both chemical and physical adsorption mechanisms.

Keywords: Oyster chitosan, Mussel chitosan, Biosorbent, Fractal-like kinetic models, Oily wastewater, Phenol, Colour.

INTRODUCTION

Industrial oily wastewater, primarily generated by petroleum refining, petrochemical processing and various manufacturing operations, has become a significant environmental concern. This type of industrial wastewater is characterized by the presence of oil droplets, grease and hydrocarbons, which can exist in free-floating or dissolved forms as elucidated by Erfani *et al.* [1]. The discharge of untreated or inadequately treated oily wastewater into waterbodies presents serious threats to both the environment and human health. It can severely disrupt aquatic ecosystems, compromise drinking water quality and negatively impact human health, highlighting the need for effective wastewater management and treatment strategies [2]. The petroleum sector is a major contributor to oily wastewater generation. Throughout the stages of oil extraction, transportation and refining, substantial volumes of water are utilized in various industrial processes. It is estimated that approximately 80-90% of the water consumed during these operations is subsequently released as wastewater [3]. Furthermore, various industrial operations, including metal processing, food manufacturing and transportation, play a significant role in producing oily wastewater as a byproduct of their processes [4]. The composition of oily wastewater is influenced by its origin and the specific industrial processes involved. Wastewater emanating from petroleum refineries consists of a diverse array of contaminants including petroleum hydrocarbons, ammonia, phenols, sulfides and various organic and inorganic substances [5,6]. These pollutants present serious dangers to both aquatic ecosystems and human health, highlighting the critical need for effective treatment methods to reduce the environmental impact of oily wastewater.

It is important to observe that the presence of oil droplets can form a surface film on water bodies, obstructing sunlight penetration and interfering with essential aquatic processes, ultimately disturbing ecosystem balance [4]. This can result in a reduction in oxygen levels, harming aquatic life and increasing the biochemical oxygen demand (BOD_5) and chemical oxygen demand (COD) in water bodies [2]. According to Wei *et al.* [7] oily wastewater emanating from petrochemical industries is characterized by high COD ranging between 20 000 mg/L and 76 000 mg/L, BOD_5 ranging from 36.1 mg/L to 650 mg/L, total nitrogen (TN) ranging from 1200 mg/L to 2736 mg/L and oil content ranging from 600 mg/L to 2200 mg/L.

Moreover, the presence of harmful organic contaminants in oily wastewater poses long-term health effects to humans, such as carcinogenic risks and chronic diseases, as well as environmental stability [2].

The remediation of oily wastewater integrates physical, chemical and biological treatment approaches to efficiently eliminate oil and associated contaminants. Physical and chemical methods are commonly used in the treatment of oily wastewater streams, *viz.* chemical coagulation/flocculation [8], adsorption [9], integrated membrane technology [10], centrifugation [11], chemical oxidation [12] and gravity separation [13]. Available literature suggests that these conventional processes are often insufficient for treating emulsified or dissolved oil, which requires more advanced technologies. On the other hand, advanced remediation techniques for oily wastewater encompass membrane separation, advanced oxidation processes (AOPs) and biological treatment [14]. These methods enhance the removal of complex contaminants by employing selective filtration, oxidative degradation of organic pollutants and micrbial activity for biodegradation, contributing to improved wastewater purification and environmental sustainability. The membrane-based separation techniques, including ultra-filtration and nanofiltration, are highly efficient in eliminating emulsified oil droplets and fine particulate matter from wastewater [14,15]. AOPs, including photocatalytic degradation and electrochemical oxidation, effectively break down persistent organic contaminants in wastewater [16]. These methods exhibit high efficiency in reducing COD and eliminating phenolic compounds, contributing to improve the water quality and environmental protection [17]. Biological treatment approaches, including activated sludge processes and bioremediation, are employed to degrade organic contaminants in oily wastewater. These methods are economically viable and environmentally sustainable; however, pretreatment may be necessary to eliminate toxic substances that could impede microbial activity and overall process efficiency [18]. According to Medeiros *et al.* [18] and Jafarinejad [19], these treatment methods offer both economic viability and environmental sustainability; however, they require pretreatment to eliminate toxic substances that could hinder microbial processes and overall efficiency.

Relative to other treatment methods, the adsorption process is considered a more advantageous option in water treatment due to its simplified design and economic feasibility, necessitating only a modest initial investment and minimal spatial requirements for effective implementation [20]. Various bioadsorbents have been developed to effectively treat oily wastewater, *viz.*, date palm, 1330 mg-oil/g-adsorbent [21], activated date-pit, 22 mg-phenol/g-adsorbent [22], banana peels, 194 mg-oil/g-banana peel [23] and pomegranate peels, 555 mg-oil/g-adsorbent [24]. From the aforementioned studies, it is apparent that the equilibrium oil removal varies with the nature of the adsorbent. This study focuses on the treatment of oily wastewater emanating from a petrochemical company using chitosan as an adsorbent. Notably, research on the utilization of chitosan flakes as a biosorbent for the treatment of raw oily wastewater remains scarce. Chitosan was selected as a potential biosorbent on the basis that it is a natural polysaccharide derived from chitin, exhibits several physico-chemical properties that enhance its application in treating oily wastewater. The effectiveness of chitosan in oily wastewater treatment is primarily due to its high adsorption capacity, attributed to its large specific surface area and the presence of amino and hydroxyl groups, which facilitate the binding of organic and inorganic pollutants [25]. Furthermore, the cationic nature of chitosan in acidic media allows it to interact with anionic compounds, enhancing its adsorption efficiency for various pollutants [26]. Available literature suggests that chitosan is an eco-friendly and cost-effective alternative to synthetic polymers, offering a sustainable solution for wastewater treatment due to its biodegradability and low toxicity [26,27].

Furthermore, the study evaluates nonlinear traditional, modified and fractal-like adsorption kinetic models by employing the Bayesian Information Criterion (BIC) and Akaike Information Criterion (AIC) as the first case. Literature suggests that nonlinear modelling approaches yield more reliable and accurate estimations of kinetic parameters [28]. Therefore, the scientific contribution of the current study is to evaluate nonlinear kinetic models with varying model parameters aimed at studying the adsorption mechanisms for the treatment of raw oily wastewater using oyster chitosan for the removal of COD, phenol and colour as the first case.

EXPERIMENTAL

All materials used in this study were of analytical grade. Sodium hydroxide, hydrochloric acid, sodium hypochlorite and sulfuric acid were supplied by Labotec, Durban, South Africa.

Sample collection and preparation: Raw wastewater samples were obtained from the effluent stream of an oil processing facility in Durban, South Africa. Filtered samples were collected in 1 L Amber bottles to prevent photolysis and were transported in a cooler box filled with ice to sustain the biological properties of the samples. Prior to sample collection on-site, the sampling point was washed to eliminate any debris or contaminants that accumulated in the sampling line. Furthermore, samples were filtered on-site to remove debris. Table-1 presents the composition of oil refinery wastewater used in this study, with all analyses performed in triplicate and average values are reported.

TABLE-1
OIL REFINERY WASTEWATER COMPOSITION

Parameter	Units	Range
pH	–	7.05-7.8
COD	mg/L	2027-2031
Turbidity	NTU	80.1-95.5
Colour	Pt-Co	1944-1981
Phenol content	mg/L	1925-1967

Herein, oil refinery wastewater samples were collected over a period of 4 weeks, aimed at studying the variation in composition over time. The pH was measured using a pH meter model EUTECH pH 700, turbidity was measured using a turbidity meter, TB350 WL measured in nephelometric turbidity units (NTU). The COD and colour were measured using the HACH DR 3900 spectrophotometer. Phenol content was measured using the ultraviolet-visible spectrophotometer, UV-VIS DU 640.

Biosorbent synthesis: Chitosan was synthesized from the oyster and mussel waste shells collected from a seafood rest-

aurant in Durban, South Africa. The shells were cleaned with deionized water, dried, crushed into flakes and then further ground into powder. Afterward, 500 g of shell powder, consisting of crushed oyster and mussel shells, was immersed in a 1 L solution containing 5 wt.% NaOH at a controlled temperature of 100 ºC for 3 h. This process aimed to eliminate protein compounds present in the shells. The resulting deproteinized powder was then thoroughly rinsed with deionized water until a neutral pH of 7 was achieved, followed by drying at 100 ºC for 2 h. The dried deproteinized powder was soaked in a 1 L solution of 5 v/v% HCl at 100 ºC for 1 h to produce chitin, which was then rinsed with deionized water to achieve pH 7. The dried chitin powder was bleached by immersing it in a 0.135 M NaOCl solution for 24 h, followed by rinsing with deionized water until a neutral pH was achieved. The bleached chitin then underwent deacetylation to convert it into chitosan, which involved heating in a 50 v/v% NaOH solution for 2 h. Afterward, the deacetylated chitosan was rinsed with deionized water to reach a neutral pH and dried at 65 ºC for 4 h, resulting in chitosan flakes. Particle size distribution analysis produced particle sizes between 25 and 1200 μ. However, samples with a particle size of 600 μ were selected based on their predetermined ability to achieve high percentage removals for the targeted contaminants.

The degree of deacetylation (DD) of the synthesized chitosan was calculated using the linear potentiometric titration method as outlined by Czechowska-Biskup *et al.* [29]. Eqn. 1 was employed in determining the DD percentage.

$$\text{DD}\ (\%) = 2.03\left(\frac{V_2 - V_1}{m + 0.0042(V_2 - V_1)}\right) \quad (1)$$

where m is the mass of the sample in grams; V_1 and V_2 are the volumes of 0.1 M NaOH solution corresponding to the deflection points; 2.03 is the coefficient resulting from the molecular weight of chitin monomer unit; and 0.0042 coefficient resulting from the difference between molecular weights of chitin and chitosan monomer units. Furthermore, the synthesized chitosan was characterized by employing the SEM coupled with EDX and the Fourier transform infrared spectroscopy (FTIR).

Batch adsorption studies: Batch adsorption studies were conducted using the one-factor-at-a-time (OFAT) method aimed at investigating the effect of three operating parameters, *viz.* biosorbent dosage (3-15 g), contact time (5-90 min) and pH (2-10) for the removal of COD, colour and phenol from wastewater emanating from an oil refinery. The traditional jar test system was employed. Wastewater samples with a volume of 500 mL were added to 1000 mL beakers connected to a mechanical stirrer. The agitation speed remained constant at 150 rpm. At a predetermined time, samples were collected for analysis. During the course of the experiments, the pH was adjusted using 1.0 M of HCl and 1.0 M of NaOH solutions. The percentage of contaminants removed and adsorbed by the model adsorbent was computed using eqns. 2 and 3, respectively.

$$\text{Adsorption}\ (\%) = \left(\frac{C_o - C_e}{C_o}\right) \times 100 \quad (2)$$

$$q_{e,i} = \frac{V(C_o - C_e)}{m} \quad (3)$$

where C_0 and C_e is the initial concentration of adsorbate and the concentration of adsorbate in solution after adsorption at equilibrium, measured in mg/L, respectively; m is the mass of adsorbent on a dry basis measured in g; and V is the volume of the sample with the initial concentration measured in L.

Adsorption empirical models

Batch adsorption kinetics: Herein, adsorption kinetics were studied by employing the pseudo-first order (PFO) (eqn. 4), pseudo-second order (PSO) (eqn. 5), the mixed 1,2-order equation (MOE) (eqn. 6), pseudo-nth-order (PNO) (eqn. 7), fractal-like PFO (eqn. 8), fractal-like PSO (eqn. 9), fractal-like MOE (eqn. 10) and the fractal-like PNO (eqn. 11) as discussed by Hu *et al.* [30].

$$q_t = q_{e1}[1 - \exp(-k_1 t)] \quad (4)$$

$$q_t = \frac{q_e^2 k_2 t}{[k_2 q_e t + 1]} \quad (5)$$

$$q_t = q_e\left\{1 - \frac{k_1 \exp(-k_1 t)}{k_1 + q_e k_2[1 - \exp(-k_1 t)]}\right\} \quad (6)$$

$$q_t = q_e\left\{1 - \left(\frac{1}{1 + (n-1)k_n q_e^{n-1} t}\right)^{1/n-1}\right\} \quad (7)$$

$$q_t = q_e\left[1 - \exp\left(-\frac{k_{1,0}}{1-h} t^{(1-h)}\right)\right] \quad (8)$$

$$q_t = q_e\left[1 - \frac{1}{1 + \frac{q_e k_{2,0}}{1-h} t^{(1-h)}}\right] \quad (9)$$

$$q_t = q_e\left\{1 - \frac{k_{1,0} \exp\left[-\frac{k_{1,0}}{1-h} t^{(1-h)}\right]}{k_{1,0} + q_e k_{2,0}\left(1 - \exp\left[-\frac{k_{1,0}}{1-h} t^{(1-h)}\right]\right)}\right\} \quad (10)$$

$$q_t = q_e\left\{1 - \left[\frac{1}{1 + (n-1)q_e^{n-1}\frac{k_{n,0}}{1-h} t^{(1-h)}}\right]^{1/n-1}\right\} \quad (11)$$

where q_t (mg g^{-1}) and q_e (mg g^{-1}) are the amounts of adsorbate uptake per unit mass of the adsorbent at time *t* and at equilibrium, respectively; k_1 (min^{-1}) and k_2 (g mg^{-1} min^{-1}) are the PFO and PSO constants, respectively; t is the contact time in (min); n is the order of reaction; $k_{n,0}$ is the fractal-like rate constant and h is the fractal-like exponent characterizing whether a system is homogeneous [30]. In the present work, adsorption isotherm studies were not conducted, as the initial concentration of adsorbates was not manipulated due to the use of real wastewater samples.

Model evaluation: The goodness of fit for the adsorption kinetics models was evaluated by employing different statistical parameters, *viz.*, the coefficient of determination, R^2 (eqn. 12), adjusted-R^2 (eqn. 13), chi-square test, χ^2 (eqn.

14), F-test (eqn. 15), Akaike Information Criterion (AIC) (eqn. 15), the Bayesian Information Criterion (BIC) (eqn. 19) and residual sum of squares (RSS) (eqn. 20).

$$R^2 = \frac{\sum_{i=1}^{n}(q_{i,exp} - \bar{q}_{i,exp})^2 - \sum_{i=1}^{n}(q_{i,exp} - q_{i,model})^2}{\sum_{i=1}^{n}(q_{i,exp} - \bar{q}_{i,exp})^2} \quad (12)$$

$$adj.R^2 = 1 - \left[\frac{(1-R^2)(n-1)}{n-p-1}\right] \quad (13)$$

$$\chi^2 = \sum \frac{(q_{e,i\,exp} - q_{e,i\,model})^2}{q_{e,i\,model}} \quad (14)$$

$$F = \frac{(RSS_1 - RSS_2)/(df_1 - df_2)}{RSS_2/df_2} \quad (15)$$

$$AIC = n\ln\left(\frac{RSS}{n}\right) + 2p + \frac{2p(p+1)}{n-p-1} \quad (16)$$

$$\Delta AIC_i = AIC_i - AIC_{min} \quad (17)$$

$$W_i = \frac{\exp(-0.5\Delta AIC_i)}{\sum_{i=1}^{n}\exp(-0.5\Delta AIC_i)} \quad (18)$$

$$BIC = n\ln\left(\frac{RSS}{n}\right) + p\ln(n) \quad (19)$$

$$RSS = \sum_{i=1}^{n}(q_{i,exp} - q_{i,model})^2 \quad (20)$$

where $q_{i,exp}$ is the experimentally measured amount of adsorbate adsorbed per gram of adsorbent; $\bar{q}_{i,exp}$ is the average of all measured experimental values of the measured amount of adsorbate adsorbed per gram of adsorbent; $q_{i,model}$ is the predicted value by the fitted model; p is the number of model parameters; n is the number of dataset points; RSS is the residual sum of squares; df is the degree of freedom with the subscripts 1 and 2 corresponding to the simple and complex models, respectively; W_i is the dimensionless Akaike weight [31-33].

RESULTS AND DISCUSSION

Biosorbent characterization

SEM/EDX studies: Figs. 1 and 2 depict the SEM/EDX results for oyster chitosan and mussel chitosan, respectively. SEM images reveal that chitosan extracted from oyster, Fig. 1a and mussel shells, Fig. 2a, exhibits a nanoporous fibrous structure, which enhances its adsorption capabilities [34]. The morphological structure of the oyster-based chitosan exhibits a more irregular and rougher surface when compared to the mussel-based chitosan, which has a surface morphology with a smooth and short microfibre structure. The SEM results for the synthesized chitosan are congruent with the work reported by Uğurlu [35], where it was reported that the surface morphology of chitosan derived from crustacean shells is rough, porous, fibrillar with nano-fibril structures.

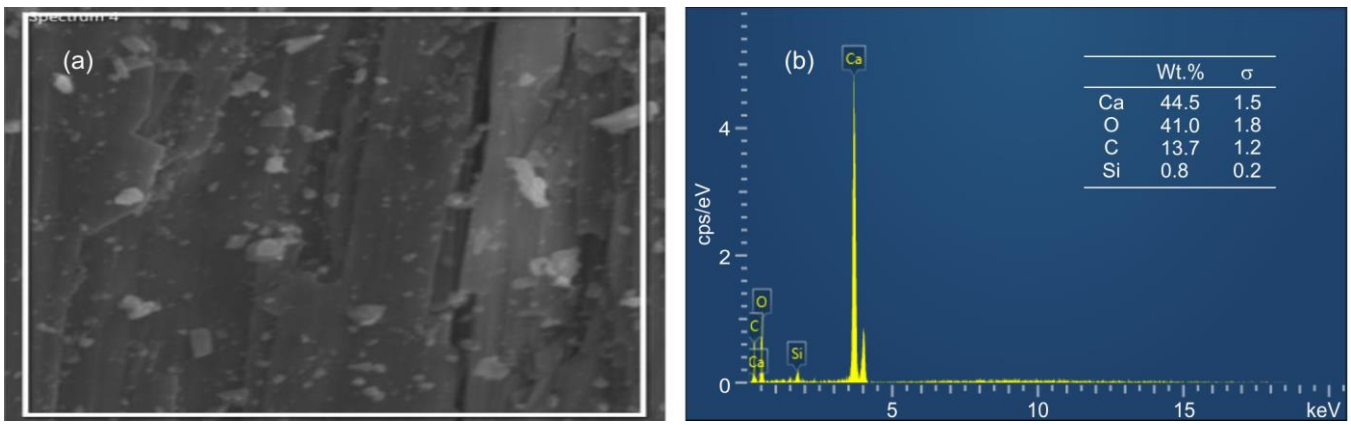

Fig. 1. SEM/EDX analysis image for oyster chitosan

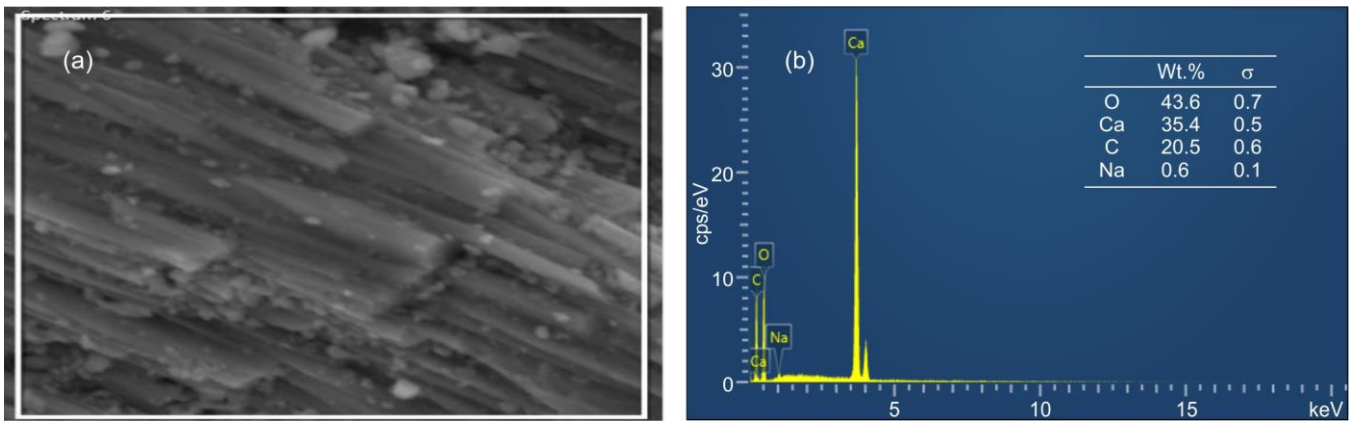

Fig. 2. SEM/EDX analysis image for mussel chitosan

Both oyster-based (Fig. 1b) and mussel-based chitosan (Fig. 2b) recorded relatively high elemental composition in terms of oxygen (O), carbon (C) and calcium (Ca). The presence of oxygen and carbon was expected, as they indicate the organic nature of the synthesized chitosan and support its suitability as a biosorbent. Carbon, in particular, enhances adsorption efficiency by offering a highly accessible surface area and forming porous structures that increase available binding sites [36]. Moreover, the intrinsic hydrophobic properties of carbon facilitate the adsorption of organic contaminants [36], potentiating the synthesized chitosan as an effective adsorbent material. On the other hand, oxygen contributes significantly to the formation of functional groups such as hydroxyl (-OH) and carboxyl (-COOH), which promote adsorption by facilitating chemical interactions with target molecules [37]. Moreover, the presence of element O increases the polarity of adsorbent, potentiating the synthesized adsorbent to be effective in the uptake of polar contaminants during the adsorption process. Similarly, the relatively high elemental composition of calcium originates from the shells of oysters and mussels [38]. The presence of calcium improves the mechanical strength of the chitosan-based adsorbent [39]. It is worth to mention that the mechanical strength of the model adsorbent was not explicitly evaluated in this study.

FTIR studies: The spectral analysis for the oyster-derived chitosan, as illustrated in Fig. 3a, indicates an absorption band at 3655 cm^{-1}, corresponding to O-H stretching vibrations, confirming hydroxyl groups presence. The peak at 2924 cm^{-1} is attributed to N-H stretching, signifying amine functionality. The vibrational mode observed at 1577 cm^{-1} validates N-H bending, further supporting the characterization of chitosan. The presence of a distinct band at 1577 cm^{-1} also suggests O=C=O bending, indicative of nano-chitosan characteristics, cementing the presence of its nanoscale structural properties. These findings are consistent with the results as previously reported by Dias *et al.* [40], affirming chitosan properties for the synthesized adsorbent.

The FTIR spectrum of mussel-derived chitosan (Fig. 3b) displays a similar overall trend to that of oyster chitosan. However, a significant difference is the lack of vibrations corresponding to the second amine group, suggesting that the chitin component was not completely removed during the extraction process. This incomplete removal indicates residual structural characteristics associated with chitin, which could affect the adsorbent's functional properties. Due to the absence of distinct amine functional groups in mussel chitosan, adsorption studies were primarily conducted with oyster-based chitosan. Oyster chitosan was used to evaluate its efficiency in removing COD, colour and phenol from wastewater produced by an oil refinery, ensuring the optimal adsorption performance.

Batch adsorption

Influence of solution pH: The pH of a solution significantly influences the behaviour and solubility of chitosan as an adsorbent, particularly in water treatment. Chitosan is insoluble in water and conventional solvents, but soluble under acidic conditions due to the protonation of its amino groups. The zeta potential test results suggest that the oyster chitosan was positively charged at a solution pH of less than 8, with its isoelectric point at 9.2 (Fig. 4a). The obtained results are attributed to the ionization of chitosan molecules, with amino groups capturing H^+ ions, resulting in a positive charge. However, as the solution pH increases, the amino groups in the synthesized chitosan were deprotonated, affecting its structural integrity by hydrogen bonding and associated forces.

From Fig. 4a, it is apparent that the adsorption performance of the synthesized oyster chitosan can be influenced by the solution pH. Fig. 4b shows the percentage removal profile of phenol, COD and colour as a function of pH. Fig. 4b shows that the removal efficiencies of phenol, COD and colour follow a similar trend with varying solution pH, with phenol demonstrating the highest removal percentage. However, beyond a pH 7, the adsorption efficiency of the model contaminants decreased. This observed pattern in phenol removal is attributed to the complex interaction between the ionization state of phenolic compounds and the electrostatic properties of the adsorbent surfaces in the solution [41]. The acidic dissociation constant (pK_a) of phenol is 9.25, indicating that at pH levels below this value, phenol predominantly exists in its neutral form, while above this pH, it dissociates to form negatively charged phenolate anions, as reported by Cui *et al.* [41]. On the other hand, the synthesized oyster chitosan exhibits positive charges at pH ≤ 8 as indicated in Fig. 4a, suggesting that the uptake of phenol was attributed to electrostatic interaction forces between the adsorbate and adsorbent. Similarly, as the solution pH increased above 7, there was a decrease in the percentage reduction of phenol, COD and colour. Similarly, in case of phenol, the observed decrease in removal efficiency can be attributed

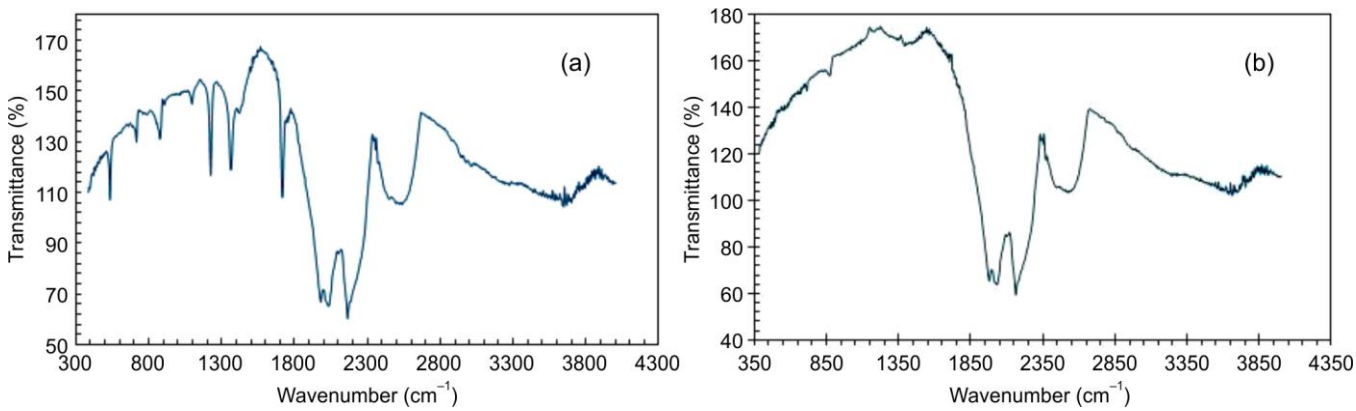

Fig. 3. FTIR spectrum for oyster chitosan (a) and mussel chitosan (b)

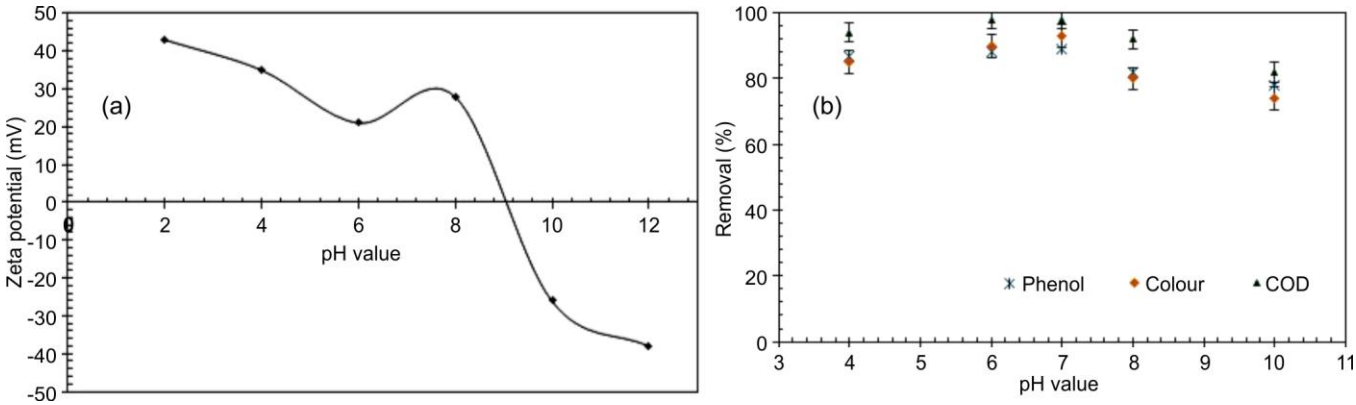

Fig. 4. Zeta potential of oyster chitosan (a) and the percentage removal profile of COD, phenol and colour as a function of solution pH (b). Operating conditions: Adsorbent dose 9 g/L, contact time 120 min and settling time 30 min

to the progressive ionization of phenolic compounds as the solution pH increases. This leads to a greater concentration of phenolate anions due to the deprotonation, thereby weakening the electrostatic interactions between the adsorbent and the adsorbate, ultimately reducing adsorption effectiveness.

Furthermore, the FTIR analysis (Fig. 3a) demonstrated that the synthesized oyster chitosan is characterised by the presence of hydroxyl functional groups. Under alkaline pH conditions, the adsorbent hydroxide ions (OH^-) and phenolic anions exert a diminishing effect on the adsorption rate due to electrostatic repulsion forces. Similarly, the COD and colour percentage reduction exhibit a similar trend with phenol, the highest percentage reductions being recorded at a solution pH of 7 for all model contaminants. The observed COD removal profile, specifically the decline in percentage removal under alkaline conditions, can be linked to the compression of the electric double layer surrounding emulsified oil droplets. This compression weakens the interfacial film, reducing its stability and promoting the disintegration and dispersion of emulsified oil into the aqueous phase, thereby influencing the overall removal efficiency [42]. This phenomenon subsequently compromised the COD uptake by the synthesized oyster chitosan. Furthermore, the relatively high COD uptake under neutral and acidic conditions can be ascribed to electrostatic interaction forces between the chitosan's positively charged amino groups and the negatively charged particulate COD [43]. Moreover, it can be observed from Fig. 4b that colour reduction exhibited a similar profile to the COD reduction profile. This suggests that the wastewater used in this study had a relatively high composition of particulate COD as opposed to dissolved COD. Based on Fig. 4b, adsorption experiments were conducted at a fixed pH of 7 on the basis that the highest removal percentage of phenol, 98%, COD, 93% and colour, 89%, were achieved at a solution pH of 7.

Effect of adsorbent dose and contact time: The adsorbent dosage and contact time are some of the critical operating parameters that can affect the adsorption process. Insufficient adsorbent dosage or contact time would result in poor performance. Fig. 5a shows the phenol, COD and colour percentage removal profile as a function of adsorbent dosage, ranging from 3 g/L to 15 g/L. From the results obtained, it can be observed that there was an increase in the percentage reduction of phenol, COD and colour with an increase in the adsorbent dose. The observed trend is attributed to the mere fact that an increase in the adsorbent dosage enhances contaminant removal due to the greater availability of active adsorption sites. Furthermore, increasing the adsorbent dosage enhances the destabilization and aggregation of oil droplets, thereby facilitating their separation. Post an adsorbent dosage of 9 g/L there was no improvement in the percentage removal of the model contaminants. While increasing the adsorbent dosage improves contaminants removal, excessive amounts may lead

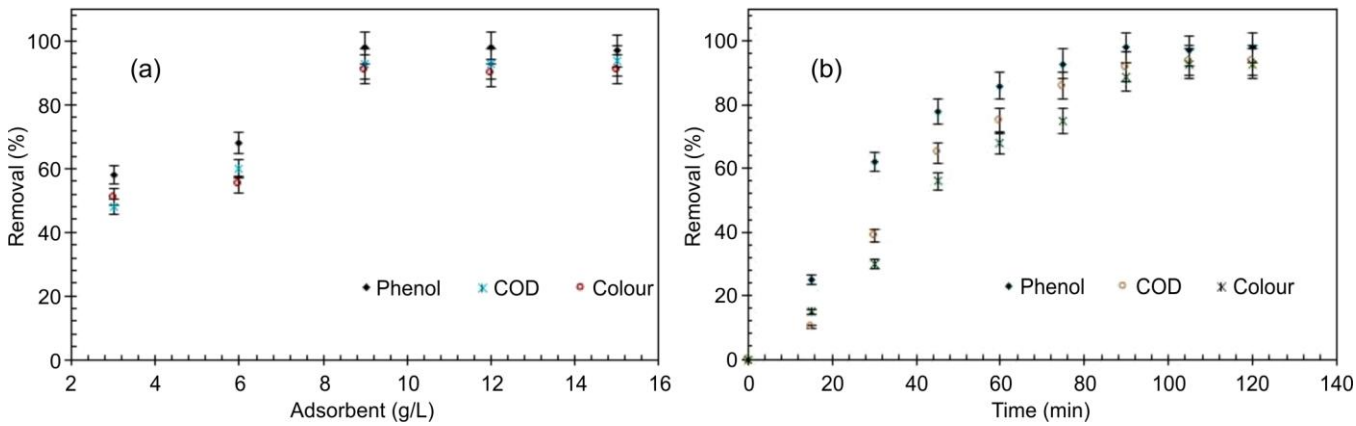

Fig. 5. Phenol, COD and colour percentage removal profile as a function of adsorbent dosage (a) and contact time (b)

to unnecessary material usage without significant gains, rendering the processing expensive.

Similarly, the findings in Fig. 5b, suggest that the treatment efficiency of oily wastewater using chitosan is significantly influenced by contact time. There was a relatively low percentage reduction in phenol, COD and colour within the first 60 min, as indicated by the error bars. The observed trend is attributed to limited adsorption due to the insufficient interactions between the chitosan adsorbent and the model pollutants. However, after 80 min of contact time, there was a relatively high percentage reduction rate on phenol, COD and colour, with the highest removal rates of 98 % phenol, 93% COD and 91% colour being recorded at a contact time of 90 min. This suggests that there was sufficient contact time between the chelating sites on the surface of the adsorbent with the model contaminants to bind effectively, thus improving the percentage reduction rate. Similarly, a further increase in the contact time post 90 min did not yield any improvement in the percentage reduction of phenol, COD and colour, as indicated by the error bars. The plateau in Fig. 5b suggests that post a contact time of 90 min, adsorption sites became saturated, which led to no further pollutant removal.

Adsorption kinetics: The experimental adsorption kinetic data were examined by fitting the generated data in different kinetic models and the results are presented in Table-2. It is apparent that all adsorption kinetic models recorded relatively high R^2 and adj.R^2 values of more than 0.9 for the uptake of phenol, COD and colour on the synthesized oyster chitosan. The R^2 parameter indicates the proportion of variability in the predicted values which is explained by the model, reflecting how closely the predictions align with the observed data. Therefore, in context of the study, a model achieves high predictive reliability when the R^2 value nears 1, indicating a strong correlation between predicted and actual data points, as reported by Montgomery [44]. A higher number of variables in the model results in an increased R^2 value, regardless of their significance. The adjusted R^2 values remain lower, as they account for the number of variables and do not increase solely with their addition. Chi-square test values below 1 were observed for all model parameters, indicating minimal discrepancy between predicted and experimental values. Despite this, the statistical parameters reported in Table-2 were not sufficient to definitively identify the kinetic model that best fit the experimental data.

On the other hand, literature [31-33,45] indicates that relying solely on R^2 and adjusted R^2 is insufficient for assessing comparative models. Instead, BIC [33] and AIC [32] are recognized as more effective metrics for assessing the model performance. When comparing models, the difference in their BIC values is a key consideration. According to Schwarz [33], if $\Delta BIC \leq 2.0$, the models exhibit no significant difference. If $2.0 < \Delta BIC < 6.0$, the model with the lower BIC value is likely more suitable. For $6 < \Delta BIC < 10$, there is strong evidence that the model with the lower BIC value is the best fit [33]. From the results presented in Table-3, in the context of phenol, the fractal-like PFO model recorded the lowest BIC value of 52.11 and the highest R^2 value of 0.9945 compared to all models investigated. Despite the lowest BIC value and relatively high R^2 value, the obtained ΔBIC values of less than 2 for the PSO and F-MOE models suggest that there is no significant difference between the PSO, F-PFO and F-MOE in fitting the phenol experimental data. Adsorption kinetic models were further evaluated by employing the AIC as a criterion for comparing adsorption kinetics, traditional, modified and fractal-like models, considering both descriptive accuracy and parsimony. Models were not selected solely based on AIC values, making it challenging to interpret the observed AIC differences in relation to a continuous measure like probability [32]. However, AIC values were transformed to the Akaike weights (w_i), which can be interpreted directly as the conditional probabilities for each model as reported by Wagenmakers & Farrell [32]. From Table-3, the traditional PSO model recorded an AIC value of 52.94 and an Akaike weight of 0.351, suggesting that the PSO model has the highest probability (0.351) of modelling the phenol experimental data accurately (Fig. 6a).

The traditional PSO model is based on the assumption that the adsorption rate of a solute is directly related to the number of available sites on the adsorbent, suggesting that the uptake of the adsorbate is dominated by chemisorption [46]. The findings of the study suggest that the uptake of phenol on the synthesized oyster chitosan is due to the formation of stronger chemical bonds between the adsorbate and the adsorbent [47]. This suggests that the sorption process of phenol on oyster chitosan is complex and involves chemisorption rather than simple physisorption. This is evident from the phenol adsorption profile as a function of the solution pH.

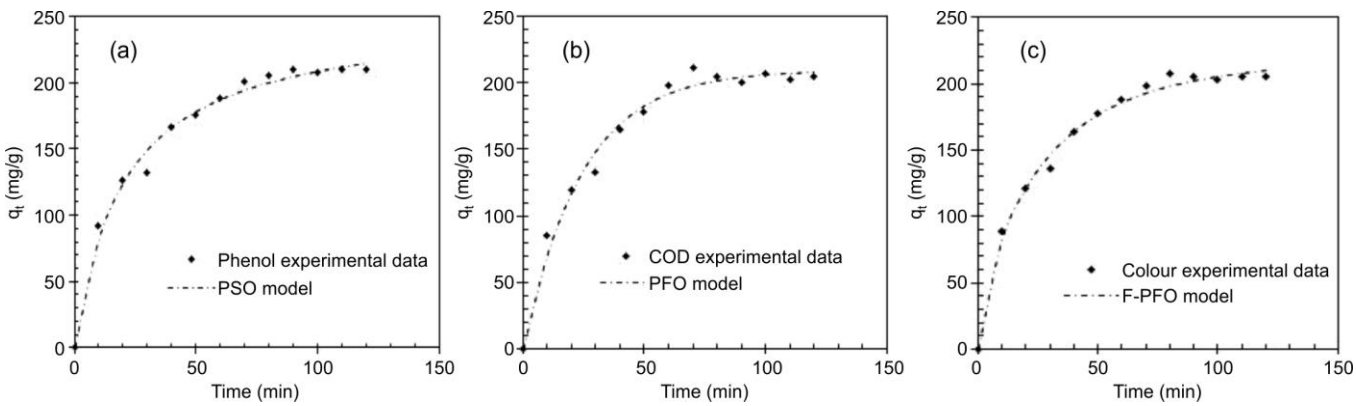

Fig. 6. Adsorption kinetic profile for phenol (a), COD (b) and colour (c). Conditions: pH 7, contact time 120 min and adsorbent dose 9 g/L

TABLE-2
ADSORPTION KINETIC PARAMETERS FOR NONLINEAR TRADITIONAL, MODIFIED AND FRACTAL-LIKE MODELS

Model type	Model	Model Parameter	Contaminant		
			Phenol	COD	Colour
Traditional model	PFO	q_{e1} (mg g^{-1})	209	209	207
		k_1 (min^{-1})	0.0414	0.0411	0.0420
		R^2	0.9804	0.9830	0.9871
		adj.R^2	0.9764	0.9797	0.9846
		χ^2	0.4292	0.3834	0.2762
Traditional model	PSO	q_e (mg g^{-1})	251	252	248
		k_2 ($g.mg^{-1}.min^{-1}$)	1.96×10^{-4}	1.896×10^{-4}	2.00×10^{-4}
		R^2	0.9890	0.9804	0.9910
		adj.R^2	0.9868	0.9765	0.9891
		χ^2	0.2409	0.4422	0.1967
Mixed 1,2 order model	MOE	q_e	250	251	247
		k_1	1.62×10^{-4}	2.02×10^{-4}	1.62×10^{-4}
		k_2	1.96×10^{-4}	1.89×10^{-4}	2.00×10^{-4}
		R^2	0.9890	0.9842	0.9910
		adj.R^2	0.9853	0.9739	0.9879
		χ^2	0.2409	0.4422	0.1967
nth-order model	PNO	q_e	275	274	269
		n	2.49	2.44	2.44
		k	1.16×10^{-5}	1.45×10^{-5}	1.56×10^{-5}
		R^2	0.9894	0.9791	0.9905
		adj.R^2	0.9859	0.9721	0.9874
		χ^2	0.2309	0.4731	0.205
Fractal-like model	F-PFO	q_e	231	214	219
		$k_{1,0}$	0.0663	0.0519	0.0617
		h	0.3025	0.1214	0.2223
		R^2	0.9945	0.9848	0.9931
		adj.R^2	0.9886	0.9797	0.9908
		χ^2	0.1865	0.3437	0.1496
Fractal-like model	F-PSO	q_e	258	252	252
		$k_{2,0}$	2.01×10^{-4}	1.89×10^{-4}	2.056×10^{-4}
		h	0.0604	0.0059	0.9910
		R^2	0.9896	0.9804	0.9880
		adj.R^2	0.9862	0.9738	0.1953
		χ^2	0.2268	0.4433	0.1953
Fractal-like model	F-MOE	q_e	226	214	217
		$k_{1,0}$	0.1967	0.1294	0.1695
		$k_{2,0}$	1.8×10^{-4}	5.1×10^{-5}	1.20×10^{-4}
		h	0.1488	0.0815	0.1201
		R^2	0.9922	0.9851	0.9936
		adj.R^2	0.9883	0.9776	0.9904
		χ^2	0.1710	0.3376	0.1385
Fractal-like model	F-PNO	q_e	322	214	220
		n	2.71	1.0	1.03
		$k_{n,0}$	2.701×10^{-6}	0.05	0.05
		h	0.1689	0.1109	0.2103
		R^2	0.9897	0.9848	0.9930
		adj.R^2	0.9845	0.9771	0.9895
		χ^2	0.2259	0.3444	0.1526

Moreover, for the uptake of COD, the traditional PFO kinetic model recorded the highest adjusted R^2 value of 0.9797 (Table-2), suggesting that the COD experimental data were better fitted by the traditional PFO with the minimal deviation from the mean. Similarly, the PFO recorded the lowest BIC value, favouring the PFO model; however, the BIC difference of less than 2 between the PFO, PSO and F-PFO models suggests that these models exhibit an insignificant difference in fitting the COD experimental data [33]. On the other hand, the PFO recorded the lowest AIC value of 58.90 and the highest Akaike weight of 0.49, suggesting that the PFO was the preferred model to fit the COD experimental data with minimal error, as depicted in Fig. 6b. It is observed that the PFO model assumes that the rate of occupation of adsorption sites

TABLE-3
MODEL VALIDATION STATISTICAL PARAMETERS

Contaminant	Parameter	Traditional		Modified		Fractal-like			
		PFO	PSO	MOE	PNO	F-PFO	F-PSO	F-MOE	F-PNO
Phenol	BIC	60.38	52.87	55.44	54.89	52.11	54.65	53.55	57.17
	ΔBIC	8.27	0.76	3.33	2.78	0	2.54	1.44	4.30
	AIC	60.45	52.94	56.41	55.86	53.08	55.63	56.29	59.91
	Wi	0.008	0.351	0.062	0.082	0.328	0.092	0.066	0.011
COD	BIC	58.83	60.69	63.25	64.13	59.97	63.28	62.31	62.57
	ΔBIC	0	1.85	4.42	5.30	1.14	4.45	3.48	3.74
	AIC	58.90	60.76	64.22	65.10	60.95	64.26	65.05	65.31
	Wi	0.49	0.20	0.03	0.02	0.18	0.03	0.02	0.02
Colour	BIC	54.65	50.09	52.65	53.21	49.10	52.65	50.66	51.92
	ΔBIC	5.56	0.99	3.55	4.12	0	3.47	1.56	2.82
	AIC	54.72	50.16	53.62	54.19	50.07	53.54	53.40	54.66
	Wi	0.03	0.34	0.06	0.05	0.35	0.06	0.07	0.04

is proportional to the number of unoccupied sites. Herein, the ability of the PFO model to fit COD experimental data suggests that physical adsorption was the dominant uptake mechanism, with the weak van der Waals forces being responsible for the interaction. Interestingly, the findings of the study presented in Tables 2 and 3 suggest that the experimental data for colour removal were better fitted by the F-PFO as depicted in Fig. 6c, recording an adjusted R^2 value of 0.9908 and an Akaike weight of 0.35.

Based on the traditional PFO model, the F-PFO kinetic model integrates the fractal theory to better represent surface heterogeneity and diffusion limitations. For colour reduction, the local heterogeneity factor (h) was determined to be 0.2223, falling within the expected range of $0 \leq h \leq 1$ and indicating a good correlation between the experimental data and the fractal-like kinetic model [48]. Therefore, the F-PFO kinetic model suggests that the adsorption sites on the synthesized oyster chitosan are not uniformly distributed. Instead, they exhibit a fractal-like structure, meaning that the adsorbent surface has a complex geometry that can be self-similar at different scales. This suggests that system complexity influences the interaction between molecules and the adsorbent, a factor not explicitly addressed in the present work. The strong correlation of the F-PFO kinetic model with experimental data, despite minimal error, implies that the adsorption process involves several transport mechanisms diffusion through the fluid phase, migration to the adsorbent surface, and eventual capture at active sites [49]. While the traditional PFO model assumes the adsorption rate is proportional to the number of available sites [49], the F-PFO model refines this assumption to reflect the dynamic nature of adsorption in complex and heterogeneous systems.

On the other hand, regardless of the relatively high R^2 and adjusted R^2 values recorded for the PNO model and MOE, the model evaluation parameters suggest that these models were not favoured to correlate the experimental data. Several studies have examined the kinetic data of various adsorption systems using the PFO and PSO adsorption kinetic models, comparing results such as kinetic parameters and deviations as reported by Tseng *et al.* [28]. Some data fit better with the PSO model, others with the PFO kinetic model, while certain cases show no significant difference between the two, indicating that the suitability of each model may vary depending on the specific adsorption conditions. This indicates that adsorption kinetic models may follow an order beyond just first or second, allowing for a more precise representation of kinetic behaviour. The idea of the PNO kinetic model was hence suggested [50]. Herein, the F-PNO kinetic model recorded n values of 1.0 and 1.03 for the sorption of COD and colour, respectively, suggesting that the COD and colour adsorption mechanisms follow the first-order. This agrees with the PFO and F-PFO kinetic models as the preferred models based on the results presented in Table-3. Moreover, for phenol, the F-PNO model recorded a value of 2.71 for n, suggesting that the uptake of phenol follows an order of 2.71, which is dissimilar with the statistical results presented in Table-3, with a deviation of 0.71 from the preferred second order, by the PSO. The F-PNO model represents an advanced kinetic approach for describing adsorption processes at the solid-liquid interface, offering improved insight into complex adsorption dynamics [51]. This model accounts for the complexity and heterogeneity of adsorption sites, making it more accurate than the traditional PNO. This is evident from the n values obtained by the F-PNO, which are closer to the preferred models as compared to the n values obtained by the traditional PNO model (Table-2).

Similarly, the F-MOE recorded relatively high R^2 and adjusted R^2 values when compared to the traditional MOE, however, the applied model evaluation criteria did not favour these models. With that being said, the BIC results for colour removal indicate that there was no significant difference between the F-MOE, F-PFO and PSO in fitting the experimental data. This is attributed to the F-MOE being an advanced kinetic model that describes adsorption at the solid-liquid interface. It integrates fractal-like kinetics with mixed PFO and PSO models to account for surface heterogeneity and complex adsorption mechanisms [48].

Khalifa *et al.* [47] conducted a study on the removal of oil from contaminated water emanating from a crude oil refinery using chitosan (*i.e.*, aminated chitosan and nonanyl chitosan Schiff base). The PFO, PSO, Elovich and Boyd adsorption kinetic models were employed to study the adsorption mechanism of the process in terms of crude oil reduction rate and the rate-limiting process. In a study conducted by Khalifa *et*

TABLE-4
KINETIC MODELS REPORTED IN THE LITERATURE FOR OILY WASTEWATER TREATMENT

Waste water source	Pollutant	Adsorbent	Kinetic fit	Removal (%)	Ref.
Crude oil refinery	Crude oil	Chitosan	Linear-PSO	–	[47]
Wastewater	Oil	CS/CA@AD	Linear-PSO	–	[52]
Crude oil refinery	Crude oil	Chitosan-rice husk as composite	Linear-PSO	96.41	[53]
Oily wastewater	Crude oil	Chitosan-Octanal Schiff base	Linear-PSO	90	[54]
Phenol-contaminated wastewater	Phenol	Chitosan-k-carrageenan hydrogel	Linear-PSO	80	[55]
Synthetic water	Phenol	Chitosan-β-cyclodextrin	Linear-PSO	96	[56]
Refinery wastewater	Phenol	Oyster chitosan	Nonlinear-PSO	98	Present study
	COD	Oyster chitosan	Nonlinear-PFO	94	
	Colour	Oyster chitosan	Nonlinear F-PFO	92	

al. [47], it was concluded that the uptake of oil on the chitosan adsorbent followed the PSO kinetic model (Table-4). The results suggest that the oil adsorption rate on chitosan is dependent on the availability of active surface sites on the adsorbent. Therefore, it was concluded that the uptake of crude oil on the chitosan-derived adsorbent was by chemical adsorption and it was the rate-limiting step in the process.

From the results presented in Table-4, it is apparent that the synthesized oyster chitosan recorded relatively high percentage reductions when compared to other chitosan-based adsorbents for the treatment of oily wastewater. Furthermore, kinetic studies of the present study suggest that the uptake of phenol on the model adsorbent follows the PSO kinetic model, which is congruent with the work reported by Hamid *et al.* [55] and Peng *et al.* [56]. Despite growing interest in wastewater treatment, studies focusing on COD and colour removal from oily wastewater are still scarce, especially those incorporating nonlinear or fractal-like kinetic modelling approaches.

Conclusion

The adsorption of phenol, COD and colour from oily wastewater using oyster-derived chitosan has proven to be an effective method. The findings of the study indicate that oyster based chitosan achieves relatively high removal efficiencies with phenol reduction reaching 96%, COD 94% and colour 92% at a solution pH of 7. These results highlight the superior adsorption efficiency of oyster-derived chitosan compared to other chitosan biosorbents, largely due to its high degree of deacetylation. It is important to note that the effectiveness of oyster-derived chitosan biosorbent is greatly influenced by the solution pH, suggesting that pollutants are adsorbed by electrostatic interaction forces. On the other hand, kinetic studies suggest that the uptake of phenol follows the PSO model, while COD and colour follow the PFO kinetic model. Therefore, it can be concluded that the treatment of oily wastewater using oyster-derived chitosan is a complex process that involves both chemical and physical adsorption. Moreover, from the model evaluation criteria employed in this study, it can be concluded that the application of R^2 and adjusted R^2 is insufficient in evaluating comparative adsorption kinetic models. However, the application of the Akaike weights can be used to successfully evaluate comparative models. The findings of the present study have demonstrated that models with more terms are not always the preferred models to correlate experimental data with minimal deviations. Therefore, it can be concluded that the application of nonlinear kinetic models can produce unbiased results. Despite the success of oyster-derived chitosan in reducing phenol, COD and colour, there is a need to conduct adsorption thermodynamic and isotherm studies to validate the uptake mechanisms as suggested by the kinetic studies presented in the current study. Furthermore, the scope of the current study does not involve the economics of the proposed adsorbent. As such, there is a need for column studies in order to perform a comprehensive technoeconomic assessment for the proposed adsorbent and its potential to be upscaled for industrial application.

ACKNOWLEDGEMENTS

The authors thank the Green Engineering Research Group at the Durban University of Technology and the Environmental Pollution and Remediation Research Group for the financial support received to conduct the study.

CONFLICT OF INTEREST

The authors declare that there is no conflict of interests regarding the publication of this article.

REFERENCES

1. H. Erfani, N.R. Madhu, S. Khodayari, M.A. Qureshi, P. Swetanshu, P. Singh and S. Jadoun, *Environ. Technol. Rev.*, **13**, 325 (2024); https://doi.org/10.1080/21622515.2024.2343129.
2. R. Abousnina, N. Ghaffour and L. D. Nghiem, *Marine Poll. Bull.*, **219**, 118240 (2025); https://doi.org/10.1016/j.marpolbul.2025.118240
3. M.S. Mansour, H.I. Abdel-Shafy and A.M. Ibrahim, *J. Environ. Manage.*, **351**, 119827 (2024); https://doi.org/10.1016/j.jenvman.2023.119827
4. S. Putatunda, S. Bhattacharya, D. Sen and C. Bhattacharjee, *Int. J. Environ. Sci. Technol.*, **16**, 2525 (2019); https://doi.org/10.1007/s13762-018-2055-6
5. S. Varjani, R. Joshi, V.K. Srivastava, H.H. Ngo and W. Guo, *Environ. Sci. Pollut. Res. Int.*, **27**, 27172 (2020); https://doi.org/10.1007/s11356-019-04725-x
6. W. Raza, J. Lee, N. Raza, Y. Luo, K.-H. Kim and J. Yang, *J. Ind. Eng. Chem.*, **71**, 1 (2019); https://doi.org/10.1016/j.jiec.2018.11.024
7. Y. Wei, Y. Jin and W. Zhang, *Int. J. Environ. Res. Public Health*, **17**, 1953 (2020); https://doi.org/10.3390/ijerph17061953
8. C. Zhao, J. Zhou, Y. Yan, L. Yang, G. Xing, H. Li, P. Wu, M. Wang and H. Zheng, *Sci. Total Environ.*, **765**, 142795 (2021); https://doi.org/10.1016/j.scitotenv.2020.142795
9. J. Odoom, O.T. Iorhemen and J. Li, *Energy Ecol. Environ.*, **10**, 15 (2025); https://doi.org/10.1007/s40974-024-00332-w

10. X.-N. Cheng and Y.-W. Gong, *Environ. Eng. Res.*, **23**, 159 (2018); https://doi.org/10.4491/eer.2016.134
11. E. Turano, S. Curcio, M.G. De Paola, V. Calabrò and G. Iorio, *J. Membr. Sci.*, **209**, 519 (2002); https://doi.org/10.1016/S0376-7388(02)00369-1
12. G. Hodaifa, P.A.R. Gallardo, C.A. García, M. Kowalska and M. Seyedsalehi, *J. Taiwan Inst. Chem. Eng.*, **97**, 247 (2019); https://doi.org/10.1016/j.jtice.2019.02.001
13. A.M. Pintor, V.J. Vilar, C.M. Botelho and R.A. Boaventura, *Clean Technol. Environ. Policy*, **16**, 1725 (2014); https://doi.org/10.1007/s10098-014-0754-3
14. D.M. Ahmed, E. Ashour and M. Shalaby, *J. Adv. Eng. Trends*, **43**, 383 (2024); https://doi.org/10.21608/jaet.2022.144929.1203
15. A. Ahmad, C. Guria and A. Mandal, *J. Water Process Eng.*, **36**, 101289 (2020); https://doi.org/10.1016/j.jwpe.2020.101289
16. M.S. Lawan, R. Kumar, J. Rashid and M.A.E.-F. Barakat, *Water*, **15**, 3676 (2023); https://doi.org/10.3390/w15203676
17. H.M. Al-Tameemi, K.A. Sukkar and A.H. Abbar, *Chem. Eng. Res. Des.*, **204**, 487 (2024); https://doi.org/10.1016/j.cherd.2024.03.004
18. A.D.L.M. Medeiros, C.J.G. Silva Junior, J.D.P. Amorim, I.J.B. Durval, A.F.S. Costa and L.A. Sarubbo, *Processes*, **10**, 743 (2022); https://doi.org/10.3390/pr10040743
19. S. Jafarinejad, Petroleum Waste Treatment and Pollution Control, Butterworth-Heinemann, pp. 185-267 (2017).
20. T.Y. Haan, P.M. Isma Nordin, N.I. Ahmad Juanda, M.A. Mohd Shafi and P. Krishnan, *Adv. Environ. Eng. Res.*, **4**, 1 (2023); https://doi.org/10.21926/aeer.2301016
21. M. Sueyoshi, R.S. Al-Maamari, B. Jibril, M. Tasaki, K. Okamura, H. Kuwagaki, H. Yahiro, K. Sagata and Y. Han, *J. Anal. Appl. Pyrolysis*, **97**, 80 (2012); https://doi.org/10.1016/j.jaap.2012.04.003
22. M.H. El-Naas, S. Al-Zuhair and M.A. Alhaija, *Chem. Eng. J.*, **162**, 997 (2010); https://doi.org/10.1016/j.cej.2010.07.007
23. U. El-Nafaty, I. Muhammad and S. Abdulsalam, *Civil Environ. Res.*, **3**, 125 (2013).
24. T.H. Ibrahim, A.S. Gulistan, M.I. Khamis, H. Ahmed and A. Aidan, *Desalination Water Treat.*, **57**, 6693 (2016); https://doi.org/10.1080/19443994.2015.1010235
25. P. Bhatt, S. Joshi, G.M. Urper Bayram, P. Khati and H. Simsek, *Environ. Res.*, **226**, 115530 (2023); https://doi.org/10.1016/j.envres.2023.115530
26. J. Desbrières and E. Guibal, *Polym. Int.*, **67**, 7 (2018); https://doi.org/10.1002/pi.5464
27. A.M. Omer, R. Dey, A.S. Eltaweil, E.M. Abd El-Monaem and Z.M. Ziora, *Arabian J. Chem.*, **15**, 103543 (2022); https://doi.org/10.1016/j.arabjc.2021.103543
28. R.-L. Tseng, P.-H. Wu, F.-C. Wu and R.-S. Juang, *Chem. Eng. J.*, **237**, 153 (2014); https://doi.org/10.1016/j.cej.2013.10.013
29. R. Czechowska-Biskup, B. Rokita, P. Ulański and J.M. Rosiak, Progress on Chemistry and Application of Chitin and its Derivatives, 20, pp. 5-20 (2015).
30. Q. Hu, S. Pang and D. Wang, *Sep. Purif. Rev.*, **51**, 281 (2022); https://doi.org/10.1080/15422119.2021.1922444
31. S.M. Khumalo, B.F. Bakare and S. Rathilal, *J. Hazard. Mater. Adv.*, **13**, 100404 (2024); https://doi.org/10.1016/j.hazadv.2024.100404
32. E.J. Wagenmakers and S. Farrell, *Psychon. Bull. Rev.*, **11**, 192 (2004); https://doi.org/10.3758/BF03206482
33. G. Schwarz, *Ann. Stat.*, **6**, 461 (1978); https://doi.org/10.1214/aos/1176344136
34. E. Uğurlu, *Biomass Convers. Biorefin.*, **15**, 25391 (2025); https://doi.org/10.1007/s13399-025-06816-x
35. E. Uğurlu, *Acta Aquat. Turcica*, **20**, 97 (2024); https://doi.org/10.22392/actaquatr.1301286
36. F. Kaya, Ş. Taşar and A. Özer, *Firat Univ. J. Exp. Comput. Eng.*, **1**, 43 (2022); https://doi.org/10.5505/fujece.2022.09797
37. I.O. Saheed, W.D. Oh and F.B.M. Suah, *J. Hazard. Mater.*, **408**, 124889 (2021); https://doi.org/10.1016/j.jhazmat.2020.124889
38. J. Gordon and E. Asiam, *Ghana Mining J.*, **16**, 42 (2016); https://doi.org/10.4314/gm.v16i2.6
39. G. Cárdenas, E. Taboada, A. Bravo and S.P. Miranda, *J. Chil. Chem. Soc.*, **48**, 49 (2003).
40. P.C. Dias, I.B. Quero, J.J. Faraoni and R.G. Palma-Dibb, *Int. J. Adhes. Adhes.*, **118**, 103215 (2022); https://doi.org/10.1016/j.ijadhadh.2022.103215
41. X. Cui, J. Liao, H. Liu, W. Tang, C. Tie, S. Tian and Y. Li, *Separations*, **10**, 523 (2023); https://doi.org/10.3390/separations10100523
42. C. Nie, G. Han, J. Ni, S. Guan, H. Du, Y. Zhang and H. Wang, *ACS Omega*, **6**, 19058 (2021); https://doi.org/10.1021/acsomega.1c02367
43. A. Ahmad, S. Sumathi and B. Hameed, *Adsorpt. Sci. Technol.*, **22**, 75 (2004); https://doi.org/10.1260/026361704323151015
44. D.C. Montgomery, Design and Analysis of Experiments, John Wiley & Sons, Inc., edn. 8 (2017).
45. E.C. Lima, F. Sher, A. Guleria, M.R. Saeb, I. Anastopoulos, H.N. Tran and A. Hosseini-Bandegharaei, *J. Environ. Chem. Eng.*, **9**, 104813 (2021); https://doi.org/10.1016/j.jece.2020.104813
46. E.D. Revellame, D.L. Fortela, W. Sharp, R. Hernandez and M.E. Zappi, *Clean. Eng. Technol.*, **1**, 100032 (2020); https://doi.org/10.1016/j.clet.2020.100032
47. R. Khalifa, A. Omer, T. Tamer, A. Ali, Y. Ammar and M.M. Eldin, *Desalination Water Treat.*, **159**, 269 (2019); https://doi.org/10.5004/dwt.2019.24166
48. H. Bashiri and A. Shajari, *Adsorpt. Sci. Technol.*, **32**, 623 (2014); https://doi.org/10.1260/0263-6174.32.8.623
49. M. Balsamo and F. Montagnaro, in eds.: G. Crini and E. Lichtfouse, Fractal-Like Kinetic Models for Fluid–Solid Adsorption; In: Green Adsorbents for Pollutant Removal: Fundamentals and Design, Springer Cham, pp. 135-161 (2018).
50. R. Leyva-Ramos, J. Rivera-Utrilla, N.A. Medellin-Castillo and M. Sanchez-Polo, *Chem. Eng. J.*, **158**, 458 (2010); https://doi.org/10.1016/j.cej.2010.01.019
51. M. Balsamo and F. Montagnaro, *Environ. Chem. Lett.*, **17**, 1067 (2019); https://doi.org/10.1007/s10311-018-00830-4
52. M.A. Ghazal, M.G. Mahmoud, I. Abed, E. Abu El-khir, M.A. Fahmy, L.A. Mohamed and A.E. Ali, *Egypt. J. Chem.*, **67**, 1693 (2024); https://doi.org/10.21608/ejchem.2024.340850.10915
53. G.G. Oseke, M.T. Isa, M.S. Galadima and A.O. Ameh, *J. Eng. Res. Reports*, **2**, 1 (2018); https://doi.org/10.9734/jerr/2018/v2i310962
54. B.Y. Eweida, A.M. Omer, T.M. Tamer, H.A.-E.M. Soliman, A.A. Zaatot and M.S. Mohy-Eldin, *Polym. Bull.*, **80**, 4813 (2023); https://doi.org/10.1007/s00289-022-04260-9
55. A.A. Hamid, J. Alam, A.K. Shukla, F.A.A. Ali and M. Alhoshan, *Int. J. Biol. Macromol.*, **251**, 126340 (2023); https://doi.org/10.1016/j.ijbiomac.2023.126340
56. H. Peng, C. Zou, C. Wang, W. Tang and J. Zhou, *Environ. Sci. Pollut. Res. Int.*, **27**, 33668 (2020); https://doi.org/10.1007/s11356-020-09437-1